IPPI
Polyolefins Journal, Vol. 3 No. 1 (2016) 47-57
ORIGINAL PAPER

# Probing into morphology evolution of magnesium ethoxide particles as precursor of Ziegler-Natta catalysts

Goond Hongmanee, Patchanee Chammingkwan, Toshiaki Taniike*, Minoru Terano

School of Materials Science, Japan Advanced Institute of Science and Technology, 1-1 Asahidai, Nomi, Ishikawa 923-1292, Japan

Received: 20 July 2015, Accepted: 6 September 2015

## ABSTRACT

$Mg(OEt)_2$ with spherical morphology is one of the most important precursors for the preparation of industrial Ziegler-Natta catalysts. In the present article, morphology evolution of $Mg(OEt)_2$ particles is studied in the course of the synthesis. The morphology of $Mg(OEt)_2$ particles is observed throughout the process by SEM. The results show that $Mg(OEt)_2$ particles are formed through i) seed generation on Mg surfaces, ii) seed growth and isolation as independent particles, and iii) further growth and shaping into smoother and more spherical particles. The size of Mg sources greatly affects the rates of these processes to different extents. A larger size of Mg leads to slower seed formation and growth, and detachment of clustered seeds, making the final particles larger and less spherical, respectively. The crystal growth of $Mg(OEt)_2$ is also affected by the size of Mg sources, which in turn differentiates the pore size distribution to affect the catalyst composition and performance. **Polyolefins J 3:47-57**

**Keywords**: Ziegler-Natta catalysts; magnesium ethoxide; morphology; polymerization; particle evolution

## INTRODUCTION

In Ziegler-Natta catalyzed olefin polymerization, polymer morphology is one of major concerns in plant production efficiency. For instance, polymer with narrow particle size distribution and high bulk density can enhance the production throughput, while inappropriate morphology can cause transportation and plugging problems [1]. It is widely accepted that the morphology of polymer replicates that of catalyst particles [2].

Polymer is generated at active sites located inside catalyst pores and accumulates hydraulic pressure, leading to particle fragmentation and exposure of new active sites. This process repeatedly proceeds in catalyst particles to yield polymer particles that imitate the catalyst morphology. To achieve well-controlled polymer morphology, intensive consideration must be paid on the catalyst design.

Nowadays, a variety of techniques have been established to control the morphology of Zielger-Natta catalysts, whose details depend on employed precursors. For instance, if adduct solution of $MgCl_2$ and ethanol is used, the solidification into desired morphology is done either by quenching after forming emulsion in inert solvent [3] or spray drying [4] prior to contacting

* Corresponding Author - E-mail: taniike@jaist.ac.jp

with $TiCl_4$. In the cases of adduct solution of $MgCl_2$ and longer alcohol (such as 2-ethyl-1-hexanol)[5] and solution of magnesium-titanium alkoxide complex [6], the solidification is often done by reaction-induced precipitation using $TiCl_4$ or other halogenating reagents, in which the morphology is tunable mainly through the reaction rate and shear force. When a pre-formed solid precursor is used, the solidification that is an essential step to obtain good particle morphology can be omitted, giving rise to a production advantage in terms of the ease of morphology control. $Mg(OEt)_2$ powder with spherical morphology is frequently selected owning to relatively high and stable activity of resultant catalysts. The morphology of catalysts is known to duplicate the morphology of $Mg(OEt)_2$ as long as the pre-formed precursor is not fragile [7]. Thus, achieving well-controlled morphology of $Mg(OEt)_2$ with sufficient particle strength is an essential step for the production of $Mg(OEt)_2$-based Ziegler-Natta catalysts.

Generally, $Mg(OEt)_2$ is synthesized from the reaction of metallic Mg and ethanol in the presence of a halide initiator. The control of particle morphology is done by optimizing synthesis conditions in an empirical way with prerequisites of narrow particle size distribution, no fine particles, sufficient particle strength and high circularity degree. It was reported that kinetics of the reaction is crucial in controlling the particle morphology, in which too fast kinetics tends to cause particle breakage and fine generation [8]. To control kinetics using Mg with an appropriate size [8], stepwise heating [9] or gradual addition of precursors [10-12] is a typical way to refine the particle size and particle size distribution. The presence of organic halide or alkaline earth metal halide produced irregular particles, while $I_2$ and magnesium halides yielded spherical particles [13, 14]. According to Tanase et al., $I_2$ increases the solubility of $Mg(OEt)_2$ by forming quasi-stable complex before precipitating into plate-like building units [13]. These building units further grow and aggregate in a hierarchical manner to form spherical macro-particles. Minor presence of certain alcohols (in addition to ethanol) can alter the shape of building units from usual plate-like to rod-like or irregular shape, affecting the sphericity of resultant macro-particles [15, 16].The particle size distribution and sphericity of $Mg(OEt)_2$ are also influenced by the morphology of Mg, in which plate-like Mg morphology leads to more spherical $Mg(OEt)_2$ particles [7]. Likewise, many ways have been empirically developed to control the morphology of $Mg(OEt)_2$ particles, while systematic understanding is still lacking on the origin of the particle morphology in the synthesis of $Mg(OEt)_2$: The majority of researchers examined the influences of certain parameters by observing the morphology of final particles without paying attention on how particles are formed and shaped in the synthesis.

In this study, the morphological development of $Mg(OEt)_2$ particles and building units was observed in the course of the reaction and the influence of Mg sources was studied in detail on the morphological development. It was found that $Mg(OEt)_2$ particles were formed through i) seed generation on surfaces of Mg, ii) isolation of growing seeds as separate macro-particles, and iii) further growth with the increase of the sphericity. The Mg sources affected the reaction rate, by which the growth and isolation processes were significantly altered. Especially, slower reaction enabled the continuous growth of both macro-particles and crystals of $Mg(OEt)_2$. Structural characteristics and ethylene/1-hexene copolymerization performance of resultant Ziegler-Natta catalysts were also studied.

## EXPERIMENTAL

### Materials

Ethanol (purity > 99.5%) was purchased from Wako Pure Chemical Industries Ltd. and dried over 3Å molecular sieves with $N_2$ bubbling for 2 h prior to use. Two types of Mg sources, denoted as MgA and MgB, were donated from Yuki Gousei Kogyo Co., Ltd. and obtained from Merck Co., Ltd., respectively. The particle size and particle size distribution from light scattering measurement were 87.8 μm and 1.48 for MgA and 278.0 μm and 0.98 for MgB. Iodine ($I_2$, purity > 99%) was used as an initiator in the $Mg(OEt)_2$ synthesis. Titanium tetrachloride ($TiCl_4$, purity > 99%) and di-n-butylphthalate (DnBP, purity > 98%) were used without further purification. n-Heptane (purity > 99.5%), toluene (purity > 99.5%) and 1-hexene (purity > 97%) were dried over 4Å molecular sieves with $N_2$ bubbling for 2 h prior to use. Triethylaluminium (TEA) used as an activator for polymerization was supplied from Tosoh Finechem Co. Ethylene of polymerization grade was donated from Sumitomo Chemical Co., Ltd.

### $Mg(OEt)_2$ synthesis

$Mg(OEt)_2$ was prepared based on a patent [10] in a 500 mL jacket-type glass reactor equipped with a mechanical stirrer. After sufficient $N_2$ replacement, the reactor was heated to 75 °C. The amount of 0.67 g of flake $I_2$ and 32.0 mL of ethanol were added into the reactor. The mixture was stirred at 180 rpm for 10 min to assure the complete dissolution of $I_2$. Then, 2.5 g of Mg and 32.0 mL of ethanol were introduced for nine times at an interval time of 10 min. After the last addition, the mixture was kept stirring for the desired aging time. The resultant solid was washed with 190 mL of ethanol twice before drying in a rotary evaporator.

The morphological development of $Mg(OEt)_2$ particles was tracked by collecting samples according to the sampling scheme in Scheme 1. 10.0 mL of suspension was taken from the reactor, and then immediately quenched in 20.0 mL of heptane at 5 °C before drying in vacuo. The samples were denoted as A (or B)-MGE010-320, in which the numeric value indicates the residence time of samples in the reactor while A or B indicates the Mg source.

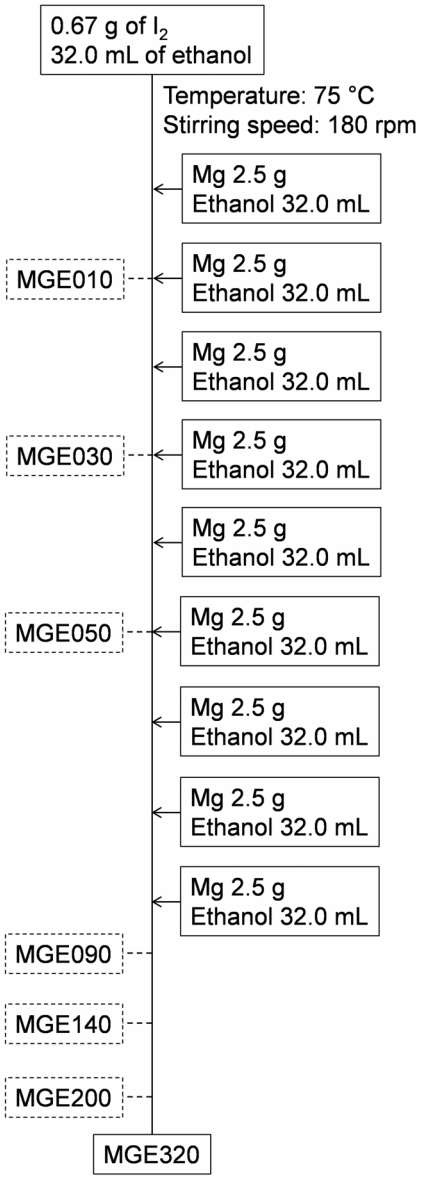


**Scheme 1.** $Mg(OEt)_2$ synthesis and sampling procedure, where the numeric values after "MGE" refer to residence time (min) in the reactor.

### Catalyst synthesis

$Mg(OEt)_2$-based Ziegler-Natta catalysts were prepared based on a patent [17] in a 500 mL three-neck round bottom flask equipped with a mechanical stirrer rotating at 180 rpm under $N_2$ atmosphere. The amount of 15.0 g of $Mg(OEt)_2$ and 150 mL of toluene were added into the flask under $N_2$ atmosphere. $TiCl_4$ (30.0 mL) was tardily dropped, where the temperature was kept at 3-5 °C. Followed by the gradual increase of temperature to 90 °C, 4.5 mL of DnBP was added. Thereafter, the reaction mixture was heated to 110 °C and stirred for 2 h. The product was washed with 150 mL of toluene twice at 90 °C and further treated with 30.0 mL of $TiCl_4$ in 150 mL of toluene at 110 °C for 2 h. Finally, the product was repetitively washed with heptane at 70 °C and at room temperature to obtain the final catalysts. Two catalyst samples, denoted as A-CAT200 and B-CAT200, were prepared from the corresponding $Mg(OEt)_2$ samples.

### Copolymerization

Copolymerization of ethylene with 1-hexene was performed in a 1 L autoclave equipped with a mechanical stirrer rotating at 750 rpm. First 500 mL of heptane and 30.0 mL of 1-hexene were introduced into the reactor under $N_2$ atmosphere. 1.0 mmol of TEA was added into the reactor, and then the solution was saturated with 0.8 MPa of ethylene at 70 °C. Then 15 mg of a catalyst was fed into the reactor to initiate the reaction. The copolymerization was conducted for 30 min at 70 °C and 0.8 MPa with the continuous feed of ethylene. Finally, the monomer was vented off and the polymer was collected and dried at 60 °C for 6 h.

### Characterization

The particle morphology of $Mg(OEt)_2$ and catalyst samples was observed by scanning electron microscopy (SEM, Hitachi S-4100) at an accelerate voltage of 20 kV. The samples were prepared under $N_2$ atmosphere, and then subjected to Pt-Pd sputtering for 60 s

before the measurement. The particle morphology in SEM micrographs was quantified using an image processing software [7]. The relative span factor (RSF) and the circularity were respectively calculated based on Equations (1) and (2),

$$\text{Relative span factor} = \frac{D_{90} - D_{10}}{D_{50}} \quad (1)$$

$$\text{Circularity degree} = \frac{4 \times \pi \times area}{(boundary \quad length)^2} \quad (2)$$

where, $D_{10}$, $D_{50}$, and $D_{90}$ correspond to the cumulative number-based particle sizes at 10%, 50%, and 90%, respectively. The area and boundary length for a two-dimensionally projected particle were determined over 500 particles. The crystal structure of $Mg(OEt)_2$ was analyzed by X-ray powder diffraction (XRD, Smart Lab., RIGAKU) using CuKα radiation at 40 kV and 30 mA. The measurement was performed based on a stepwise scanning in the range of 6-14 degree with the step of 0.1 degree per 30 s. A sample was loaded onto a glass holder under $N_2$ atmosphere, and then covered by a Mylar film to prevent the contact with moisture. The crystal size was estimated based on the Scherrer's equation [18] for each specified diffraction peak.

The pore architecture of catalysts was determined by $N_2$ adsorption/desorption measurement (BELSORP-max) at 77 K. A pyrex tube was heated at 200 °C overnight in vacuo for eliminating moisture. The amount of 50.0 mg of a catalyst was added in the pyrex tube under $N_2$ atmosphere. Then, the sample was outgassed at 80 °C for 3 h. The micropore volume (D< 2 nm) was calculated based on the previously proposed equation [7]. The mesopore volume (2 nm <D< 50 nm) was analyzed by the INNES method [19]. The chemical compositions of catalysts were measured based on previously reported procedures [7]. The Ti and donor contents were determined by UV/vis spectroscopy (JASCO V-670) and IR spectroscopy (FTIR-4100, JASCO), respectively. The n-butyl branch content in copolymer was determined by 13C NMR (Bruker 400 MHz) operating at 100 MHz at 120 °C. 1,2,4-Trichlorobenzene and 1,1,2,2-tetrachloroethane-d2 were used as solvent and an internal lock, respectively.

## RESULTS AND DISCUSSION

Morphological evolution of $Mg(OEt)_2$ synthesized using different Mg sources was tracked. Both of the Mg sources, denoted as MgA and MgB, have similar platelet morphology with smooth surfaces (Figure 1). However, the particle size of MgA was in the range of 30-100 μm, much smaller than that of MgB, whose size was in the range of 100-300 μm, in accordance to light scattering measurement. Figures 2 and 3 show SEM micrographs for A- and B-MGE, respectively. In the case of A-MGE, huge chunks having surfaces fully covered by aggregated small seeds were observed at the first 10 min of the reaction (Figure 2a). Considering the size of MgA, it was reasonable that the chunks were MgA particles with the reaction product formed on the surfaces. After the repetitive addition of the reagents, the small seeds continued to grow and transform into spherical-like particles on the surfaces (Figure 2c), followed by breakage of the chunks into clusters of spherical-like particles as well as single spherical-like particles (Figure 2e). As the reagent addition progressed (from 50 to 90 min), the spherical-like particles continuously grew and the clusters broke up into single particles (Figure 2g). The aging of reaction products (from 90 to 320 min) did not have a significant effect on the particle characteristics, except the improvement of the particle sphericity (Figures 2g,i,k,m).

In the case of B-MGE, the needle-like rods, whose presence was not detected in A-MGE, were observed at the first 10 min (Figure 3a). These rods (with the longer dimension around 30-60 μm) were mainly attached on the MgB particles. Along the repetitive addition of the reagents, these needle-like rods transformed into aggregated seeds with irregular shapes (Figure 3c). It was notable that smooth surfaces, characteristic for MgB, were still observable. At 50 min, clusters of $Mg(OEt)_2$ seeds with irregular shapes appeared (Figure 3e) as separate particles. Judging from the persistence of original MgB particles (not shown here), these clusters resulted from the detachment of aggregated seeds from the MgB surfaces. The growth

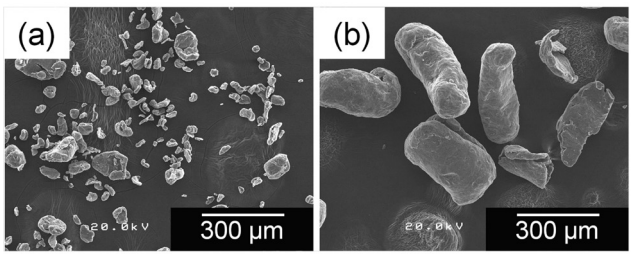


**Figure 1**. SEM micrographs of Mg powder: (a) MgA (x100) and (b) MgB (x100).

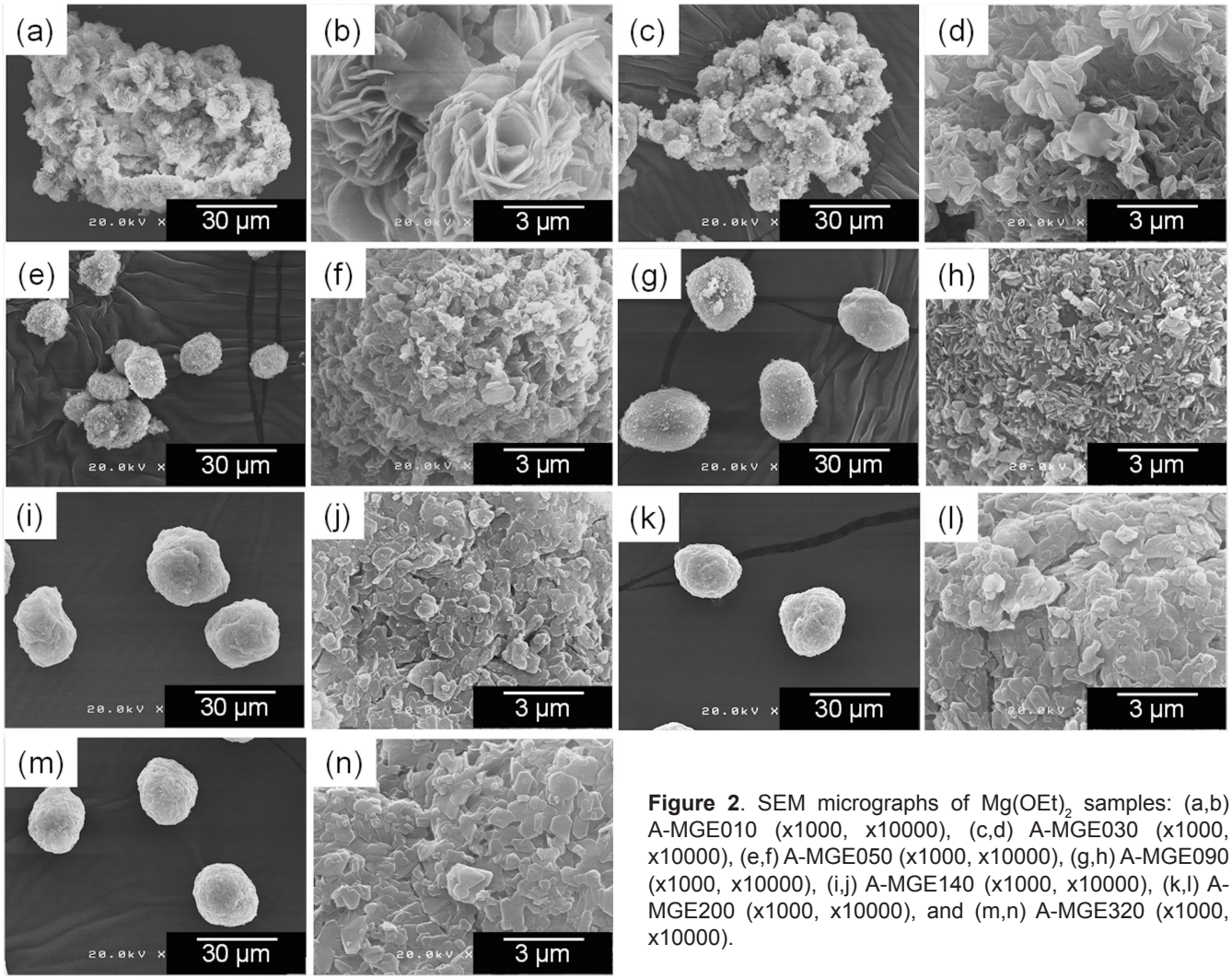


**Figure 2**. SEM micrographs of $Mg(OEt)_2$ samples: (a,b) A-MGE010 (x1000, x10000), (c,d) A-MGE030 (x1000, x10000), (e,f) A-MGE050 (x1000, x10000), (g,h) A-MGE090 (x1000, x10000), (i,j) A-MGE140 (x1000, x10000), (k,l) A-MGE200 (x1000, x10000), and (m,n) A-MGE320 (x1000, x10000).

of the detached clusters continued even in the aging (from 90 to 200 min) to reach the maximum particle size (Figure 3g,i,k). Further extension of the aging from 200 to 320 min improved the sphericity of particles without significant change in the particle size. However, fractures on the particle surfaces started to appear, which is not promising in catalyst preparation (Figure 3m).

The characteristics of $Mg(OEt)_2$ particles were acquired from SEM micrographs (Table 1). It should be noted that the image analysis was not conducted on A- and B-MGE010-030 samples, because the co-presence of irregular particles on the Mg surfaces largely misled the analysis results. In Table 1, the $D_{50}$ value of isolated (or detached) particles was found to be similar for both of A- and B-MGE050. Even though huge chunks were still observed in B-MGE050, their fraction was too small to affect the particle size calculation based on number average. The particle size increased with the increase of residence time and converged at 90 and 200 min for A- and B-MGE, where the maximum D50 values were 27 and 39 µm, respectively. The convergence of the particle sizes for A- and B-MGE indicated the complete consumption of metallic Mg, where A-MGE required shorter time to reach the consumption and to stop the growth. The smaller particle size and faster convergence for A-MGE could be ascribed to the faster reaction rate: MgA accompanied faster seed formation, thus generating a larger number of particles. In addition, MgA was more rapidly consumed, and consequently the particle growth converged at an earlier timing than that for MgB. The RSF value for both of the samples decreased with the increase of the residence time and became stable when the particles stopped obvious growth. The circularity degree increased over the addition and aging period for both of the samples, indicating that morphological shaping occurred in a continuous manner [7].

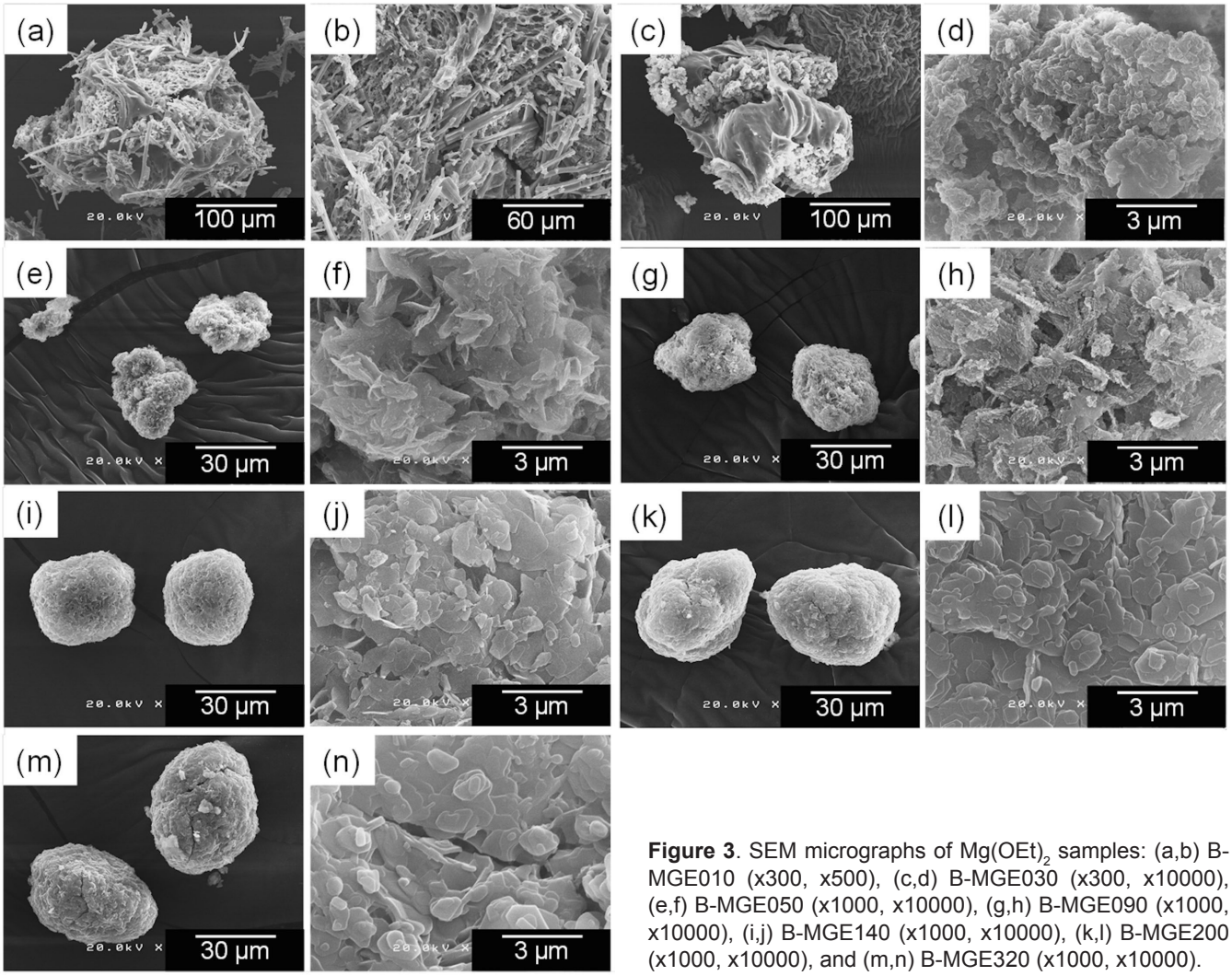


**Figure 3**. SEM micrographs of $Mg(OEt)_2$ samples: (a,b) B-MGE010 (x300, x500), (c,d) B-MGE030 (x300, x10000), (e,f) B-MGE050 (x1000, x10000), (g,h) B-MGE090 (x1000, x10000), (i,j) B-MGE140 (x1000, x10000), (k,l) B-MGE200 (x1000, x10000), and (m,n) B-MGE320 (x1000, x10000).

Whilst the morphological development of $Mg(OEt)_2$ particles was more or less similar for the two Mg sources, the morphology of building units was quite unique, especially during the reagent addition period. The large micron-sized platelets were firstly observed for A-MGE (Figure 2b) before converting into much smaller building units having irregular shapes and sizes (Figures 2d,f,h). In the case of B-MGE, the needle-like rods were firstly formed (Figure 3b) and subsequently experienced several morphological transformations (Figures 3d,f,h). Finally, the plate-like building units, which are typically observed for $Mg(OEt)_2$, were formed during the aging period (at 140 min) for both of A- and B-MGE and persevered upon extending the aging time (Figures 2i,l,n and 3j,l,n). These observations revealed that the evolution of building units into the stable form went through several metastable forms, whose pathway was dependent on the Mg sources.

**Table 1**. Particle characteristics of $Mg(OEt)_2$

| | $D_{10}$[(a)] (µm) | $D_{50}$[(a)] (µm) | $D_{90}$[(a)] (µm) | RSF[(b)] | Circularity[(c)] |
|---|---|---|---|---|---|
| A-MGE050 | 12.4 | 18.3 | 38.9 | 1.448 | 0.746 |
| A-MGE090 | 21.7 | 26.8 | 41.8 | 0.750 | 0.822 |
| A-MGE140 | 22.4 | 27.2 | 42.9 | 0.754 | 0.833 |
| A-MGE200 | 21.8 | 26.3 | 41.1 | 0.734 | 0.849 |
| A-MGE320 | 20.5 | 25.3 | 40.2 | 0.779 | 0.893 |
| | | | | | |
| B-MGE050 | 12.9 | 19.8 | 29.5 | 0.838 | 0.683 |
| B-MGE090 | 15.9 | 27.3 | 38.0 | 0.809 | 0.774 |
| B-MGE140 | 16.8 | 30.6 | 46.2 | 0.961 | 0.761 |
| B-MGE200 | 27.5 | 39.3 | 48.5 | 0.534 | 0.823 |
| B-MGE320 | 23.2 | 38.3 | 47.5 | 0.634 | 0.855 |

(a) $D_{10}$, $D_{50}$, and $D_{90}$ are the particle diameters at 10%, 50% and 90% in the cumulative number-based particle size distribution obtained by the analysis of SEM micrographs over 500 particles.
(b) Determined based on Equation (1).
(c) Determined based on Equation (2).

From the SEM micrographs, the particle evolution was found to be consistent with a scheme previously proposed by Tanase et al. [13] $Mg(OEt)_2$ seeds were initially formed on Mg surfaces and subsequently detached due to the collision and other shear force. The isolated particles continued to grow further from the precipitation of quasi-stable $n$Mg(OEt)$_2$.MgI$_2$.$m$EtOH soluble complex. This mechanism holds regardless Mg sources (ribbon or powder form). However, it is interesting to address that the isolation of seeds was greatly affected by the Mg sources. A-MGE was mainly isolated as single particles, while B-MGE was predominantly isolated as clusters (Figures 2e and 3e). This difference was believed to be relevant to the reaction rate. MgA offered a higher reaction rate, thus seeds could be rapidly developed as single particles before the isolation. On the contrary, the seed formation and growth of B-MGE particles were much slower and seeds were detached as clusters. The subsequent aging helped to gradually improve the circularity. However, the final circularity was still influenced by the morphology of initially isolated particles, in which higher circularity was obtained when the seeds were isolated as single particles. Our findings are summarized in Scheme 2.

The crystal structure of $Mg(OEt)_2$ during the reaction was observed by XRD and the results are shown in Figure 4. A-MGE010 exhibited a single broad peak, demonstrating that the initially formed seeds were poorly crystalline. Thereafter, several diffraction peaks appeared in the 2$\theta$ range of 8-12 degree, indicating the formation of crystal phases. As designated in Figure 4, the intensity of peaks in the regions I, III, V, VI, VIII and IX decreased with the increase of the residence time and the peaks finally disappeared at 140 min. At the same time, the intensity of peaks in the regions II, IV and VII gradually increased and became dominant during the aging period. In the case of B-MGE, the XRD patterns in the initial stage were different from those of A-MGE. B-MGE010 exhibited a sharp main peak positioned in the region V. At 30 min, this peak completely disappeared, while the broad peak between the regions I and II started to develop. The co-existence of several peaks between regions III-VIII was also recognized for B-MGE030-090 samples. The XRD patterns of B-MGE eventually became similar to those of A-MGE at 140 min, where the three main characteristic peaks in the regions II, IV and VII became dominant. The appearance and disappearance of several peaks along the residence time specified the co-presence of different crystal phases, especially during the repetitive addition of the reagents in the initial stage. The transformation of XRD peaks synchronized well with the transformation of building units in SEM micrographs. It was deduced that the unique morphology of building units in the initial stage might correspond to the metastable forms (MGE010-090). Accordingly, the plate-like building units with the crystal structure typical for $Mg(OEt)_2$ plausibly corresponded to the stable form (MGE140-320). The difference in the reaction rate between MgA and MgB was believed to alter the composition of $n$Mg(OEt)$_2$.MgI$_2$.$m$EtOH soluble complex, resulting in the formation of different metastable forms [20]. The formation of the stable phase induced the undersaturation of solution with respect to the metastable phases, which resulted in the

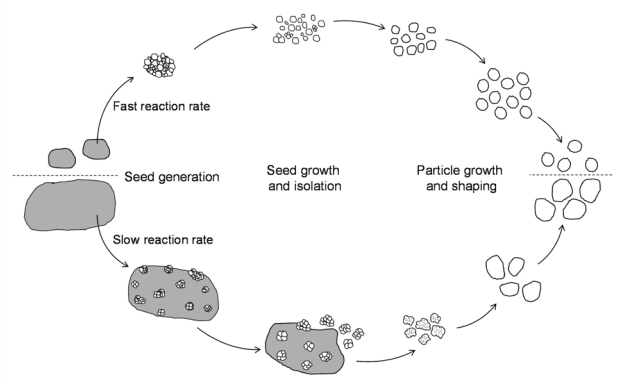


**Scheme 2.** Mg(OEt)2 particle formation and evolution.

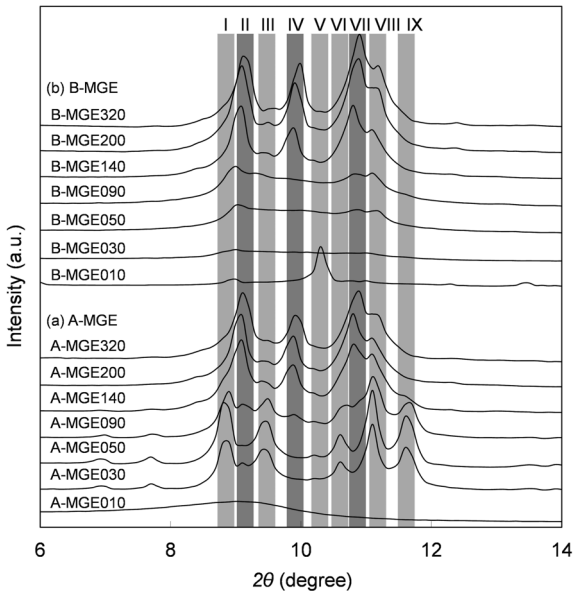


**Figure 4**. XRD patterns of $Mg(OEt)_2$: (a) A-MGE and (b) B-MGE.

gradual disappearance of metastable phases [21].

The crystal size of the stable phase was calculated from the three main peaks (in the regions II, IV and VII) using the Scherrer's equation (Figure 5). Even though the crystal phase was similar, the dimension of crystal was different. The crystal size of A-MGE exhibited significant difference for the three peaks, while B-MGE exhibited similar sizes. The aging increased the crystal size for both of the samples. However, the crystal size for A-MGE converged at the residence time of 200 min, while no convergence of the crystal size was found for B-MGE within 320 min of the reaction. It should be noted that the particle size was converged earlier than the crystal size (at 90 min for A-MGE and at 200 min for B-MGE), suggesting that the repining process continued even after the particles stopped obvious growth.

According to our previous works, the pore architecture of $Mg(OEt)_2$-based catalysts was essentially decided by the structural characteristics of $Mg(OEt)_2$[15, 16]. Therefore, the influence of the Mg sources was investigated on the pore characteristics of catalysts. $Mg(OEt)_2$ samples with the residence time of 200 min were chosen to ensure not only the complete conversion of Mg, but also the best balance in terms of the $Mg(OEt)_2$ morphology. A- and B-MGE200 samples were converted into catalysts and denoted as A- and B-CAT200, respectively. SEM micrographs in Figure 6 exhibit that the morphology of both catalysts replicates that of original $Mg(OEt)_2$ except the molten edges and smoother surfaces, which are generally observed for $Mg(OEt)_2$-based Ziegler-Natta catalysts [7]. Note that no fine particles were observed after catalyzation for both of the samples, indicating the adequate physical stability of both samples.

The $N_2$ adsorption/desorption isotherms of the catalysts are shown in Figure 7. Both of the catalysts exhibited similar adsorption isotherms, classified as type II in IUPAC for macroporous solid [22]. The hysteresis loop of type H3 in IUPAC classification indicated slit-shape mesopores, whose size and shape were non-uniform [22]. The pore size distributions are shown in Figure 8. In both of the catalyst samples, the pore distribution exhibited bimodal characteristics typically observed for $Mg(OEt)_2$-based Ziegler-Natta catalysts [15]. The micropore volume was found to be similar for both of the Mg sources. This is in accordance with our previous work, where the micropores were believed to derive from the volumetric shrinkage during catalyzation and insensitive to the variation of $Mg(OEt)_2$ synthesis conditions [15]. Meanwhile, the meso-pore volume was found to be smaller for B-CAT200. The suppression of meso-pore volume of B-CAT200 is yet unknown. However, in considering characteristics of B-MGE compared to A-MGE, this difference might be relevant to the smaller and more uniform crystal size for B-MGE.

The compositions of catalysts are reported in Table 2. B-CAT200 contained the lower Ti and donor contents compared to A-CAT200, while the molar ratio between donor and Ti was similarly kept at 1.6. This result indicated the competitive adsorption between Ti and donor [23], which was not affected by $Mg(OEt)_2$ structural differences. Thus, the lower Ti and donor contents in B-CAT200 was believed to originate from the smaller pore volume, i.e. smaller surface area of original B-MGE200.

Ethylene/1-hexene copolymerization was performed to investigate the performance of catalysts, especially for the insertion ability of relatively large monomer. The catalytic activities and *n*-butyl branch contents are reported in Table 2. The activity per Ti-mol was found to be similar for both of the catalysts. Contrary, the 1-hexene incorporation efficiency for B-CAT200 was slightly lower than that for A-CAT200, which attributed to the suppression of mesopore volume [7].

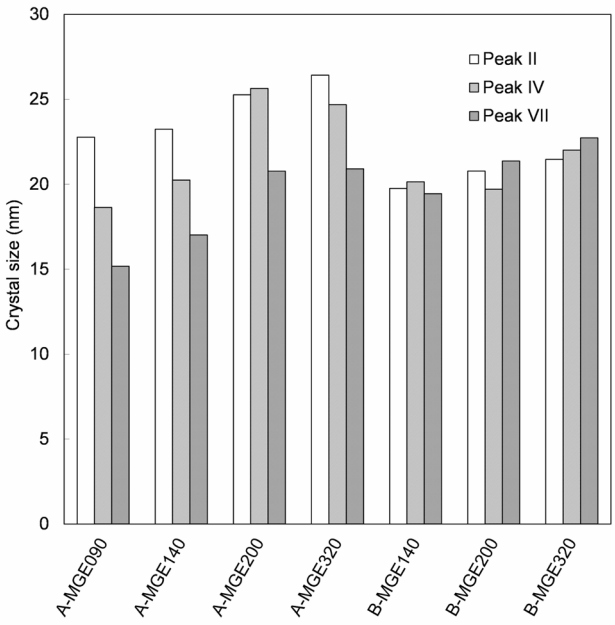


**Figure 5**. Calculated crystal sizes based on specified diffraction peaks for A- and B-MGE.

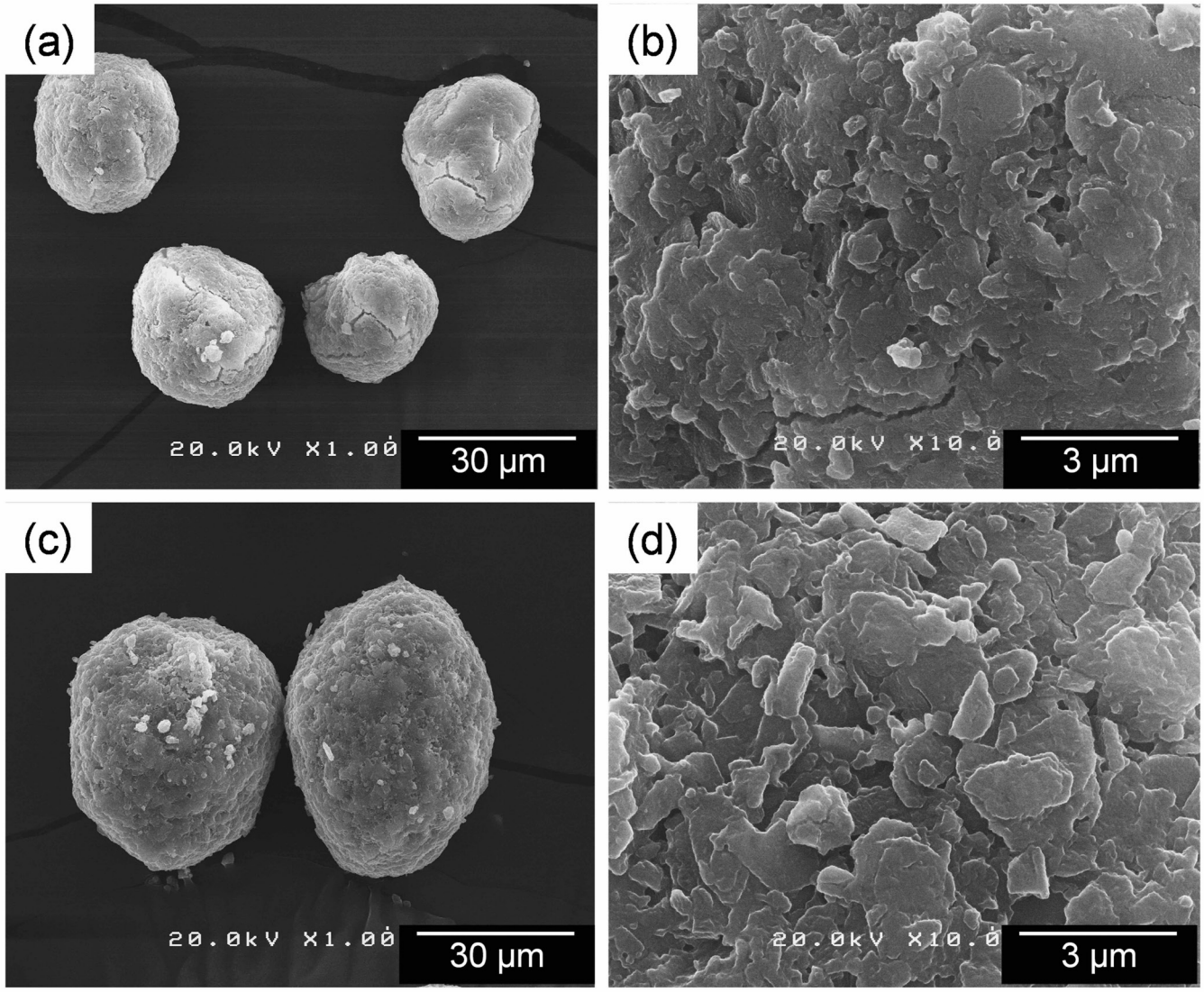


**Figure 6**. SEM micrographs of catalyst particles: (a,b) A-CAT200 (x1000, x10000) and (c,d) B-CAT200 (x1000, x10000).fibers.

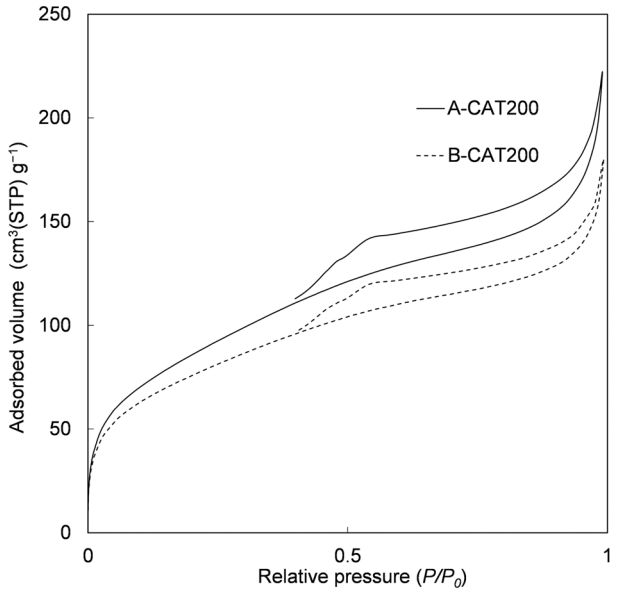


**Figure 7**. $N_2$ adsorption/desorption isotherms for catalyst samples.

## CONCLUSION

The influence of Mg sources on the evolution of $Mg(OEt)_2$ particles was investigated by observing the morphology of $Mg(OEt)_2$ particles during the synthesis. We found that Mg sources influenced not only the growth of initially formed seeds, but also the detachment behavior of growing seeds. The smaller size of Mg offered a higher reaction rate, resulting in the rapid development of seeds into spherical-like $Mg(OEt)_2$ particles on Mg surfaces, which were afterward isolated as single particles. The morphology of the isolated particles determined the sphericity of $Mg(OEt)_2$ particles, even though subsequent aging gradually improved it. Mg sources also influenced the morphology of $Mg(OEt)_2$ building units as well as the crystal growth, differentiating the pore size distribution of catalysts (mainly for meso-pores). The mesopore

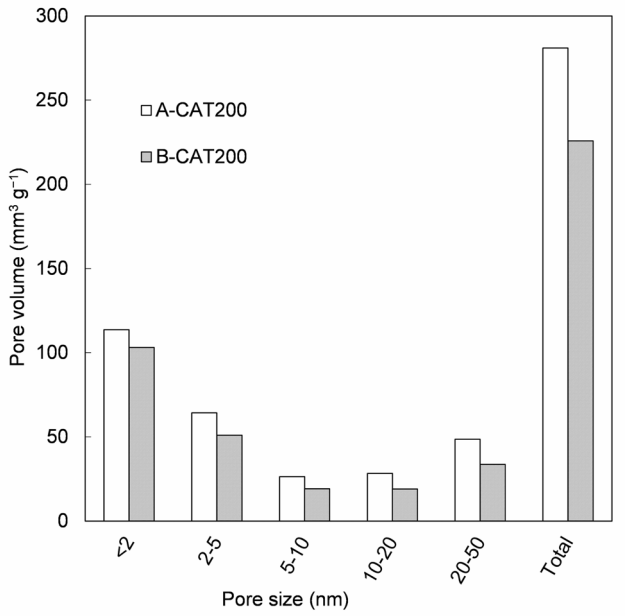


**Figure 8**. Pore size distribution of catalyst samples.

volume of the catalysts became larger when $Mg(OEt)_2$ was prepared using the smaller size of Mg, and caused enhanced comonomer incorporation in ethylene/1-hexene copolymerization. Thus, the present study has successfully clarified the origin of the morphology of $Mg(OEt)_2$ particles in a comprehensive manner, which must contribute to finer design of the morphology and performance of Ziegler-Natta catalysts.

## ACKNOWLEDGEMENTS

The Authors appreciate Sumitomo Chemical Co., Ltd., Toho Titanium Co., Ltd., Tosoh Finechem Co. and Yuki Gousei Kogyo Co., Ltd. for the reagent donation.

**Table 2**. Chemical compositions and polymerization results

| | Ti content[(a)] (wt%) | Donor content[(b)] (wt%) | Activity[(c)] (kg-polymer Ti-mol $^{-1}h^{-1}atm^{-1}$) | n-Butyl branch content[(d)] (mol%) |
|---|---|---|---|---|
| A-CAT200 | 2.8 | 17 | $3.3 \times 10^3$ | 0.75 |
| B-CAT200 | 1.8 | 11 | $3.2 \times 10^3$ | 0.56 |

(a) Determined by UV/vis spectroscopy.
(b) Determined by FTIR.
(c) Ethylene/1-hexene copolymerization was conducted at 70 °C in 500 mL of heptane with 1.0 mmol of TEA, 0.2 mol of 1-hexene, and 0.8 MPa of continuously supplied ethylene for 30 min.
(d) Determined by $^{13}C$ NMR.

## REFERENCES

1. Pater JTM,Weickert G, Van Swaaij WPM (2003) Polymerization of liquid propylene with a fourth-generation Ziegler–Natta catalyst: Influence of temperature, hydrogen, monomer concentration, and prepolymerization method on powder morphology. J Appl Polym Sci 87: 1421-1435
2. Galli P, Barbè PC, Noristi L (1984) High yield catalysts in olefin polymerization. General outlook on theoretical aspects and industrial uses. Angew Makromol Chem 120: 73-90
3. Ye ZY, Wang L, Feng LF, Gu XP, Chen HH, Zhang PY, Pan J, Jiang S, Feng LX (2002) Novel spherical Ziegler–Natta catalyst for polymerization and copolymerization. I. Spherical $MgCl_2$ support. J Polym Sci, Part A: Polym Chem 40: 3112-3119
4. Miya S, Tachibana M, KarasawaY (1992) Process for producing a catalyst for olefin polymerization. US Patent 5100844
5. Kioka M, Kitani H, Kashiwa N (1982) Process for producing olefin polymers or copolymers. US Patent 4330649
6. Batinas-Geurts AA, Friederichs NH, Schoffelen T, Zuidema E (2014) Catalyst system for the production of ultra-high molecular weight polyethylene. US Patent 20140296454
7. Taniike T, Funako T, Terano M (2014) Multilateral characterization for industrial Ziegler-Natta catalysts toward elucidation of structure-performance relationship. J Catal 311: 33-40
8. Joseph J, Singh SC, Gupta VK (2009) Morphology controlled magnesium ethoxide: Influence of reaction parameters and magnesium characteristics. Part Sci Technol 27: 528-541
9. Gupta V, Singh S, Makwana U, Joseph J, Singala K, Rajesh S, Patel V, Yadav M, Singh G (2014) Spheroidal particles for olefin polymerization catalyst. US Patent 8633124B2
10. Nomura H, Kurihara N, Higuchi K (1991) Synthesis of spherical magnesium alcoholate having narrow particle size distribution. JP Patent 199174341
11. Yamanaka A, Kumai H, Suyama M (2007) Dialkoxymagnesium granular material and synthesis and use thereof. JP Patent 2007297371
12. Yamanaka A, Kumai H, Suyama M (2014) Dialkoxymagnesium granules and method for their synthesis. US Patent 8632882
13. Tanase S, Katayama K, Inasawa S, Okada F, Yamaguchi Y, Konakazawa T, Junke T, Ishihara N (2008) Particle growth of magnesium alkoxide as a

carrier material for polypropylene polymerization catalyst. Appl Catal A: Gen 350: 197-206
14. Tanase S, Katayama K, Inasawa S, Okada F, Yamaguchi Y, Sadashima T, Yabunouchi N, Konakazawa T, Junke T, Ishihara N (2008) New synthesis method using magnesium alkoxides as carrier materials for Ziegler-Natta catalysts with spherical morphology. Macromol React Eng 2: 233-239
15. Funako T, Chammingkwan P, Taniike T, Terano M (2015) Alternation of pore architecture of Ziegler–Natta catalysts through modification of magnesium ethoxide. Macromol React Eng. DOI: 10.1002/mren.201400074
16. Funako T, Chammingkwan P, Taniike T, Terano M (2015) Addition of a second alcohol in magnesium ethoxide synthesis as a way to vary the pore architecture of Ziegler-Natta catalysts. Polyolefins J 2: 65-71
17. Terano M, Murai A, Inoue M, Miyoshi K (1987) Catalyst for polymerization of olefin. JP Patent S62158704
18. Scherrer P(1918) Determination of the size and internalstructure of colloidal particles using X-rays. Math-Phys Kl 2: 98-100
19. Innes WB (1957) Use of parallel plate model in calculation of pore size distribution. Anal Chem 29: 1069-1073
20. Turova NY, Turevskaya EP (1972) Alkoxymagnesium halides. J Organomet Chem 42: 9-17
21. Snyder RC, Doherty MF (2007) Faceted crystal shape evolution during dissolution or growth. AIChE J 53: 1337-1348
22. Leofanti G, Padovan M, Tozzola G, Venturelli B (1998) Surface area and pore texture of catalysts. Catal Today 41: 207-219
23. Potapov AG, Bukatov GD, Zakharov VA (2009) DRIFTS study of the interaction of the $AlEt_3$ cocatalyst with the internal donor ethyl benzoate in supported Ziegler–Natta catalysts. J Mol Catal A: Chem 301: 18-23